Monthly Notices
of the
ROYAL ASTRONOMICAL SOCIETY

MNRAS **491,** 2129–2136 (2020)
Advance Access publication 2019 November 14

doi:10.1093/mnras/stz3128

Extended main sequence turnoffs in open clusters as seen by *Gaia* – II. The enigma of NGC 2509

M. de Juan Ovelar [1]★ S. Gossage,[2] S. Kamann [1] N. Bastian,[1] C. Usher [1] I. Cabrera-Ziri,[2]† A. Dotter,[2] C. Conroy[2] and C. Lardo [3]

[1]*Astrophysics Research Institute, Liverpool John Moores University, 146 Brownlow Hill, Liverpool L3 5RF, UK*
[2]*Harvard-Smithsonian Center for Astrophysics, 60 Garden Street, Cambridge, MA 02138, USA*
[3]*Laboratoire d'astrophysique, Ecole Polytechnique Fédérale de Lausanne (EPFL), Observatoire de Sauverny, CH-1290 Versoix, Switzerland*

Accepted 2019 November 3. Received 2019 October 16; in original form 2019 August 13

ABSTRACT

We investigate the morphology of the colour–magnitude diagram (CMD) of the open cluster NGC 2509 in comparison with other Galactic open clusters of similar age using *Gaia* photometry. At ∼900 Myr Galactic open clusters in our sample all show an extended main sequence turnoff (eMSTO) with the exception of NGC 2509, which presents an exceptionally narrow CMD. Our analysis of the *Gaia* data rules out differential extinction, stellar density, and binaries as a cause for the singular MSTO morphology in this cluster. We interpret this feature as a consequence of the stellar rotation distribution within the cluster and present the analysis with MESA Isochrones and Stellar Tracks (MIST) stellar evolution models that include the effect of stellar rotation on which we based our conclusion. In particular, these models point to an unusually narrow range of stellar rotation rates ($\Omega/\Omega_{\rm crit,\,ZAMS} = [0.4, 0.6]$) within the cluster as the cause of this singular feature in the CMD of NGC 2509. Interestingly, models that do not include rotation are not as good at reproducing the morphology of the observed CMD in this cluster.

Key words: techniques: photometric – open clusters and associations: general.

1 INTRODUCTION

Originally discovered in massive intermediate-age stellar clusters in the Large Magellanic Clouds (Mackey & Broby Nielsen 2007), extended main sequence turnoffs (eMSTOs) are now known to be a common feature of clusters with ages between 10–20 Myr (Li et al. 2017; Beasor et al. 2019) and ∼2 Gyr (e.g. Martocchia et al. 2018) and masses as low as a few thousand solar masses (e.g. Piatti & Bastian 2016). Additionally, with proper motion cleaned high precision photometry available with *Gaia*, eMSTOs have been seen in an increasing sample of Galactic open clusters as well (Bastian et al. 2018; Cordoni et al. 2018; Marino et al. 2018).

The ubiquity of the eMSTO feature, as well as the observed relation between the age of the cluster and the extent of the MSTO width (Niederhofer et al. 2015), argues for a stellar evolutionary effect as the cause of the feature. One such effect could be stellar rotation, where rotating stars have their position in a colour–magnitude diagram (CMD) shifted due to changes in both their internal chemical and hydrostatic equilibrium structures (Bastian & de Mink 2009). Indeed, the position of a star within the CMD on the MSTO has been found to be correlated with the measured rotational velocity ($V \sin i$) in a number of clusters (Dupree et al. 2017; Bastian et al. 2018; Kamann et al. 2018; Marino et al. 2018).

As part of a large study on the eMSTO phenomenon, we have compiled a list of ∼50 open clusters with precise parallax determination, low differential extinction, and with ages that span from ∼30 Myr to ∼4 Gyr. The full sample and analysis will be presented in a future work (de Juan Ovelar et al., in preparation). As part of this analysis, we found a specific cluster, NGC 2509, which deserves special attention, given its apparent lack of an eMSTO at an age (∼900 Myr) where all other coeval clusters in the sample clearly show it. In this study, we analyse the CMD of NGC 2509 and compare it with other clusters in our sample with similar ages using photometry obtained with *Gaia*. In particular, we compare the eMSTO properties of NGC 2509 to NGC 1817, NGC 2360, NGC 2818, NGC 5822, NGC 7789, and Melotte 71, focusing on its lack of eMSTO in comparison with the others. We argue that the particular morphology of NGC 2509's MSTO is related to the particulars of its member's rotation distribution.

In Section 2, we present the data and the process followed to select members of the clusters, and to estimate their extinction, ages, and age spread. In Section 3, we analyse NGC 2509's CMD in comparison with the other clusters, and in Section 4, we discuss the possible explanations of the differences we find. Finally, we present our conclusions in Section 5.

★ E-mail: m.dejuanovelar@ljmu.ac.uk
† Hubble fellow.

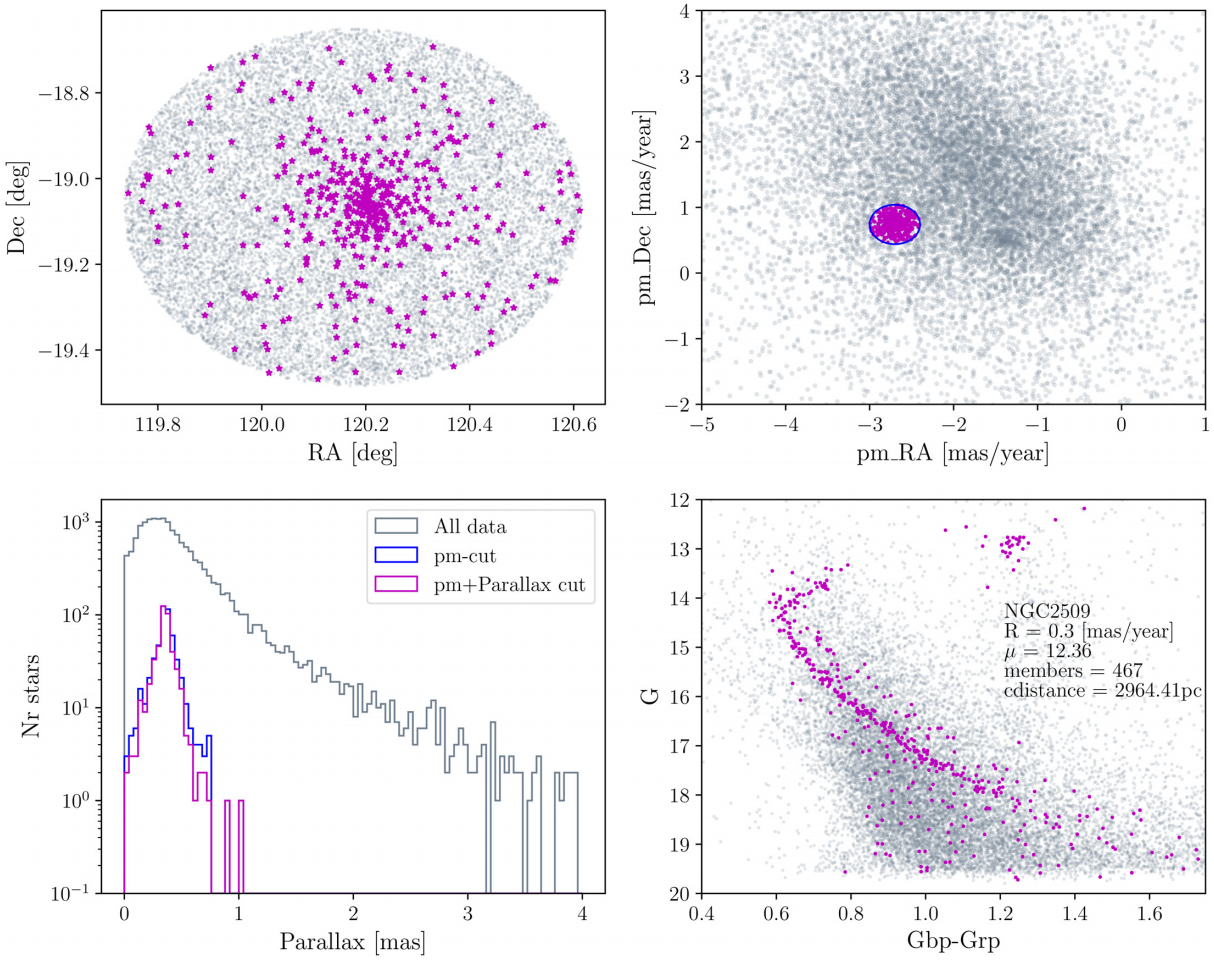

Figure 1. Top left: spatial distribution of the stars in the *Gaia* catalogue within 10 arcmin of NGC 2509's centre (hereafter referred to as field of view). Cluster members are highlighted as magenta filled stars. Top right: proper motions of all stars, with cluster members shown as magenta filled dots. The blue circle marks the area occupied by the selected members in proper motion space. Bottom left: parallax distribution of all stars in the field of view (grey solid line), stars within the proper motion area we defined for the cluster (blue solid line), and selected members based on the proper motions and parallax cuts applied (see Section 2.1). Bottom right: colour–magnitude diagram (CMD) of all stars in the field with cluster members shown again as magenta filled dots.

2 DATA AND METHODOLOGY

2.1 Membership selection

We use *Gaia* Data Release 2 (DR2) data of the following clusters: NGC 1817, NGC 2360, NGC 2509, NGC 2818, NGC 5822, NGC 7789, and Melotte 71. These clusters are those in our sample with clean CMDs and ages within 200 Myr of ∼900 Myr, which is our estimated age for NGC 2509. We downloaded *Gaia* DR2 astrometry, proper motions, photometry, and parallaxes of stars within 10 arcmin of the centre of each cluster.

The cluster member selection is done systematically as follows. First we clean the downloaded catalogue by rejecting sources with an error in proper motion larger than 0.5 mas yr^{-1}. We then determine the cluster centre either by means of a 2D histogram of the remaining stars in proper motion space, or by directly inspecting the proper motion diagram. Then, we select stars within a certain radius of this centre in proper motion space, which is different for each cluster, and build a histogram of their parallaxes. Any star with parallax value within $2\sigma_t$ of the maximum of the parallax distribution, with σ_t being each individual star's error in parallax, is considered a candidate member. At this point, we refine the selection applying a further 3D membership probability cut in proper motion and parallax space following the method outlined in Kamann et al. (2014) and assuming a velocity dispersion of 2 km s^{-1} independently of the cluster.

Fig. 1 shows images of spatial, proper motion, parallax, and colour–magnitude distributions for the cluster NGC 2509 used to select the cluster members (top left-, top right-, bottom left-, and bottom right-hand panels, respectively). Once we have a catalogue of members for each cluster, we obtain an estimate of the cluster distance d by computing the median value of the parallax of all members above a G magnitude of 17. We then obtain the distance modulus (μ) of each cluster as $\mu = 5 \times \log(d) - 5$. In order to investigate the effect that the zero-point offset issues in the *Gaia* parallaxes (e.g. Lindegren et al. 2018) have in our μ values, we have recomputed all distance moduli in our sample subtracting 0.08 mas from the median parallax measured for each cluster, which is the maximum average global offset we found in the literature (see Choi et al. 2018). The average variation in the values of μ for our sample is of a 3.3 per cent, with a maximum of 5.8 per cent for the cluster NGC 2818. Keeping in mind that we assumed the worst-case scenario for a global offset in parallax, we can assume that the impact of this issue in our particular sample is very low.

Table 1. Estimated parameters for our cluster sample.

Cluster	μ	A_V	Age	Δ_{MSTO}	$N^{\star}_{MS}$	f_{bin}	$r_{MSTO/MS}$
NGC 1817	11.37	1.1	720	230	140	0.17	3.36
NGC 2360	10.23	0.5	960	370	101	0.21	3.79
NGC 2509	12.36	0.75	860	60	116	0.17	1.38
NGC 2818	12.82	0.9	720	230	179	0.19	3.27
NGC 5822	9.63	0.6	810	202	91	0.18	4.18
NGC 7789	11.76	1.3	1070	390	736	0.19	2.41
Melotte 71	11.81	0.65	940	210	184	0.16	3.77

Note. Cluster, distance modulus, extinction, age (Myr), main sequence turnoff (MSTO) spread (Myr), number of stars in main sequence (MS) subsample, binary fraction (observed, see text), and ratio of standard deviation of distribution of distances to line A in MSTO subsample over standard deviation of distribution of distances to line B in MS subsample (see text and Fig. 3).

2.2 Estimating extinction and age

In order to estimate the extinction (A_V) and age of the clusters, we first fit non-rotating MESA Isochrones and Stellar Tracks (MIST) isochrones (Choi et al. 2016; Dotter 2016) with a range of ages (from 10 Myr to 10 Gyr) to the main sequence (MS) region of the CMD using A_V as a free parameter. We then proceed to find the two isochrones delimiting the MSTO's blue and red edges ($\log(\mathrm{Age})_{min}$ and $\log(\mathrm{Age})_{max}$, respectively), which we then use to define the spread of the MSTO (Δ_{MSTO}) as the difference (in Myr) between the two isochrones. We finally compute the age as the middle point between these two delimiting isochrones (again in Myr). The values obtained for the parameters of each cluster are shown in Table 1. Fig. 2 shows our age fit for NGC 2509 as an example. Note that all of the isochrone fitting is done visually, and so we expect some differences between the values found in this study and those across the literature. However, it is important to note too that the absolute values we find through this method are not very relevant to the study since our analysis and statistics are done in relative terms, i.e. comparing cluster's CMD morphologies directly (see next section).

Following this isochrone fitting procedure, we find an age for NGC 2509 of 860 Myr, and a MSTO spread of 60 Myr. Note that this value for the MSTO spread is very low compared to the other clusters in our sample that, with ages 900 ± 200 Myr, all present spreads of at least 200 Myr (see Table 1). In particular, the two clusters closest in age to NGC 2509, i.e. Melotte 71 (940 Myr) and NGC 5822 (810 Myr), have spreads of 210 and 202 Myr, respectively.

3 ANALYSIS

Because the ages and age spreads we obtain with the above procedure are dependent on a visual fitting of isochrones, we choose to compare the CMDs between clusters directly. Fig. 3 shows the result of this procedure for all clusters included in this study, with the left-hand panel showing the CMDs of all clusters, once corrected for extinction and distance using A_V and the distance modulus (μ), overplotted in different colours. We then select cluster members in the MSTO by means of a cut in their colour and magnitude. In particular, we select members of all clusters with colour ($G_{bp} - G_{rp}$) and magnitude (G) values between [0.1–0.6] and [1.5–0], respectively. Then we compute the distances, in CMD space, of each member in this region to an arbitrary line that we fix for all clusters (blue line A in left-hand panel of Fig. 3). In this way, we are able to build a distribution of distances that gives us an idea of the spread of the MSTO subsample and allows us

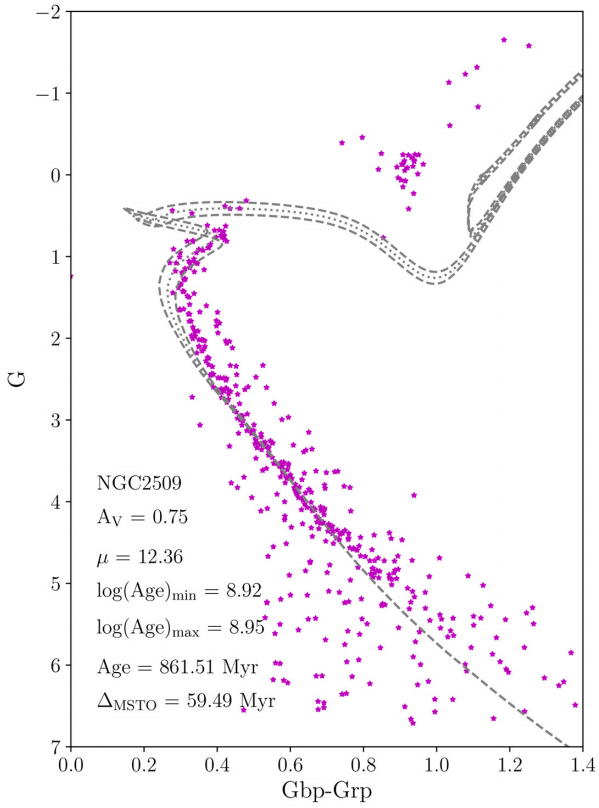

Figure 2. Colour–magnitude diagram (CMD) of NGC 2509's cluster members shown as magenta filled stars. Three non-rotating MIST isochrones are shown together with the data. The two grey dashed lines correspond to the isochrones delimiting the spread of the main sequence turnoff (MSTO) in NGC 2509 (Δ_{MSTO}). The grey dotted line is the nearest isochrone to our estimated age.

to compare the morphology of the MSTO of each cluster directly. The normalized histograms and kernel density estimates (KDEs) of these distribution are shown in the upper right-hand panel of Fig. 3 for all clusters. The histograms, shown as filled bars, are computed using 10 bins for all clusters. The KDEs, shown as solid lines, are computed using Gaussian kernels and Scott's 'rule of thumb' bandwidth selection method. Note that the histograms and KDEs are computed independently from each other. Because of the small differences in age between clusters, the distributions are slightly misaligned, so we correct for that aligning their peaks (or centres, in the case of bimodal distributions) with the peak in the MSTO distribution of NGC 2509. This operation is just for visualization purposes and does not affect the shape of the distribution. In this panel, we can already see that the MSTO of NGC 2509 (solid magenta line) is significantly narrower than the MSTOs of the other clusters in the sample.

In order to verify that the differences in the morphology of these MSTO distributions are not caused by e.g. differential extinction that could be broadening the CMD of each cluster differently, we repeat this procedure on stars in the MS region of the CMD, selecting those with colour and magnitude values between [0.3–0.8] and [3.8–2.3], respectively, and defining a new, fixed, line in that region (orange line B in left-hand panel of Fig. 3) and compute the distance. We build the corresponding histograms and KDEs in the same way we did for the MSTO region. The result of this analysis is shown in the lower right-hand panel of Fig. 3, where it is

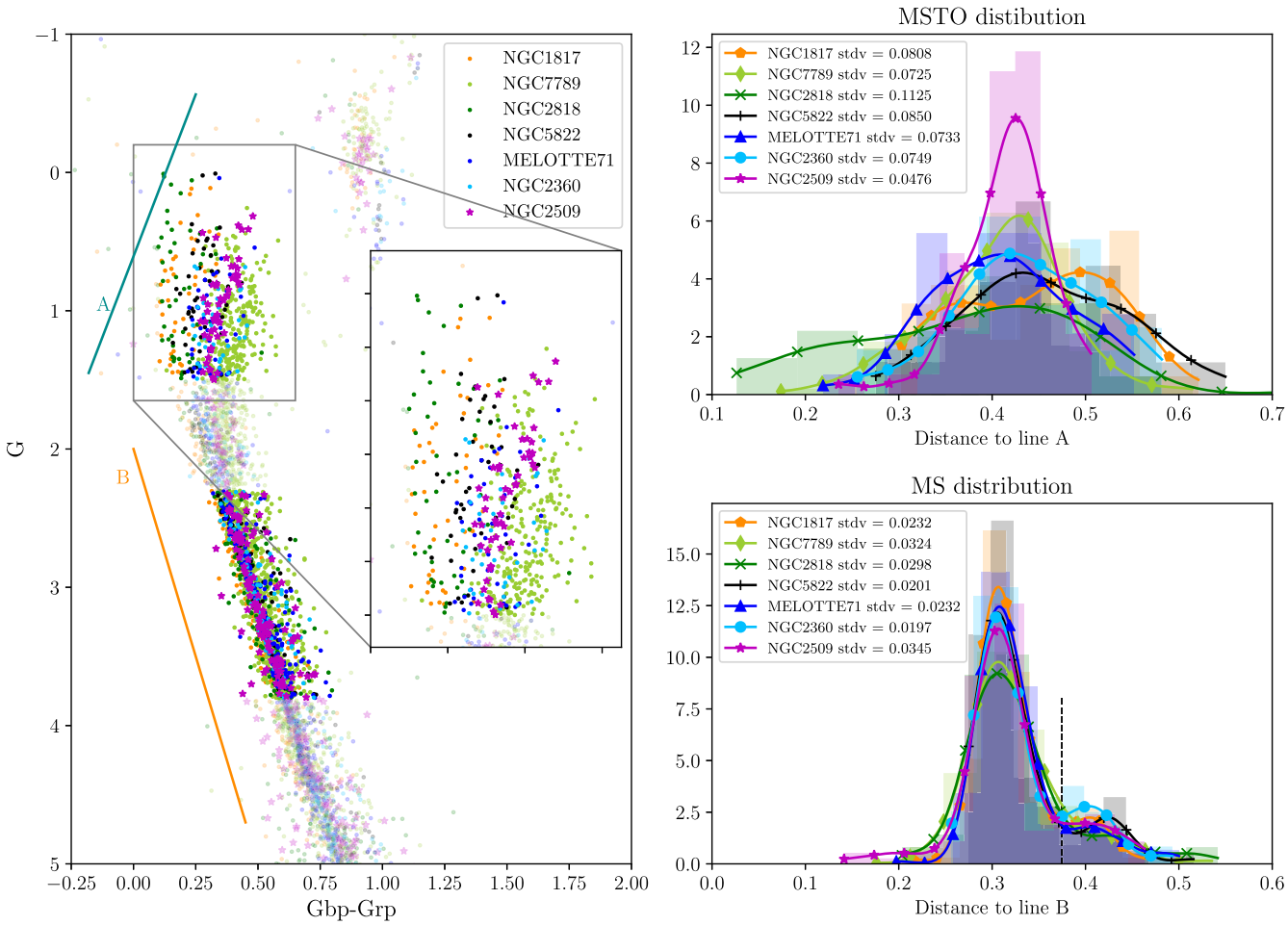

Figure 3. Left-hand panel: colour–magnitude diagram (CMD) of all clusters included in this study shown as colour coded filled dots except for NGC 2509 that is shown in magenta filled stars. The blue and orange solid lines designated as A and B are the lines used for the analysis of the main sequence (MS) and main sequence turnoff (MSTO) regions of each cluster's diagram (see Section 3). A detail of the MSTO region of the diagram is shown in the zoomed-in inset. Upper right: histograms and Kernel Density Estimates (KDEs) computed for the distributions of distances of stars in the MSTO regions of each cluster to the line A. Lower right: same as the upper panel but computed for the distributions of distances in the MS region to line B. Note that solid-fill symbols highlight the members selected to represent these two regions. The vertical black dashed line marks the separation we define between stars in the MS (to the left of the line) and stars in the binary sequence of the clusters. The legend in each of these two right-hand panels shows the computed standard deviations of the distributions, which, in the case of the MS region (lower right-hand panel), excludes all stars in the binary sequence, i.e. those to the right of the vertical black dashed line.

clear that the distributions, their widths in particular, are remarkably similar, ruling out the possibility of external factors (i.e. differential extinction) being the cause of the differences seen in the MSTO region. In order to quantify this difference we compute standard deviations of all distributions of distances. The ratio between the MSTO distribution's standard deviation to the MS one gives an idea of how much more the MSTO is broadened with respect to the MS. This ratio for NGC 2509 is of ∼1.4, while the minimum ratio found in the rest of the sample clusters is ∼2.4 for NGC 7789, with a maximum of ∼4.2 for NGC 5822. This gives an idea of how different NGC 2509 is from the rest of the sample. Note that we excluded what we identified as the binary sequence of our clusters[1] from the standard deviation calculation in the MS region. The effect of binaries in the broadening of the MSTO is not significant (see Section 4.3) so in this region we include the full range of the distribution.

Finally, in order to rule out differential extinction as a MSTO broadening factor in particular, we performed an experiment to measure its effect. We created synthetic clusters using the same non-rotating and solar metallicity MIST isochrones with no differential extinction we use for the age fitting procedure. We then add a range of values for differential extinction (0.0–0.3) and we run our method on them. We then measure standard deviations in the same way as we did for our observed clusters and compute the ratios in MSTO standard deviation to MS one for the distribution of distances in the two regions of each cluster. We found a maximum ratio of 1.8 in the worst differential extinction case (0.3). Note that these synthetic clusters do not have binaries. The ratios obtained for our observed clusters are much larger, which effectively rules out differential extinction as a possible cause for the differences we are finding between NGC 2509 and the rest of clusters in our sample.

[1]We define as the binary sequence distribution, the part of the distances distribution in the MS region to the right of the vertical black dashed line in the lower right-hand panel of Fig. 3.

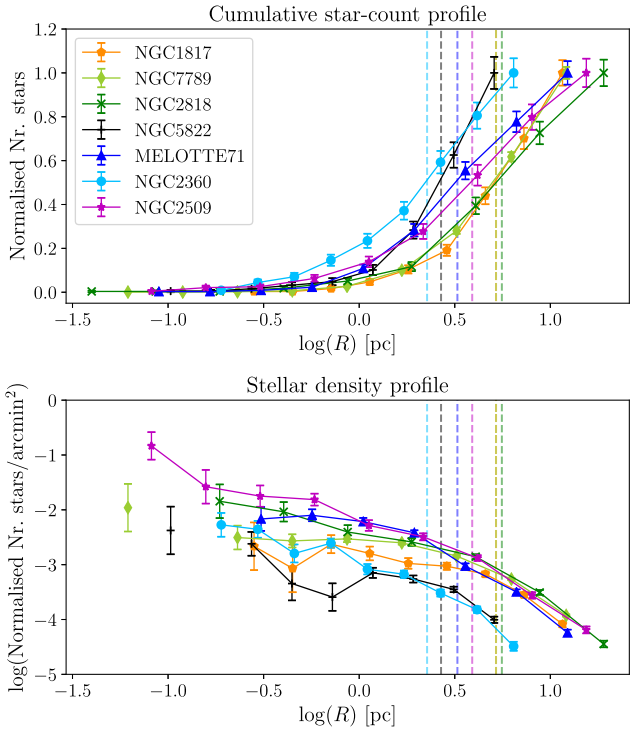

Figure 4. Upper panel: cumulative star counts profile of the cluster members colour coded for each cluster. The vertical dashed lines mark the half-light radius of each cluster. Lower panel: stellar density profiles of the clusters.

4 DISCUSSION

We have shown that the open cluster, NGC 2509, has a much narrower MSTO than all other clusters in our survey with similar ages. The question, naturally, becomes why is this the case? In order to answer this question we have looked at a number of things that could affect the spread in the MSTO region of the CMD in these clusters.

4.1 Stellar density

One potential cause for the differences between NGC 2509 and the other clusters could be if the clusters' stellar densities are significantly different (as this may affect the rotational distribution of stars). Fig. 4 shows the radial cumulative star counts and stellar density profiles (top and bottom panels, respectively) of all clusters included in this study. We can see here that NGC 2509 does not stand out as particularly special in terms of density.

In order to further confirm this, we estimate the relative densities of all clusters in our samples using the number of stars used to fit the width of the MS region ($N^{\star}_{\rm MS}$ in Table 1) as a proxy for mass, and our estimates for the half-light radius of each cluster (dashed coloured lines in Fig. 4). Our choice of method to approximate the mass of the clusters is justified by the fact that the MS region is complete for all clusters and also has relatively small errors (on proper motions and parallax) so that background contamination is minimized. With these estimates for the relative density of the clusters we find that all clusters in our sample have similar densities within a factor of 5. This rules out density as a cause for the lack of eMSTO in NGC 2509. So next, we look at the rotation distribution within the cluster.

4.2 Stellar rotation distribution

In studies of the eMSTO phenomenon, the case has been made for a distribution of rotation rates as the cause behind the phenomenon (e.g. Bastian & de Mink 2009; Brandt & Huang 2015; Niederhofer et al. 2015; Kamann et al. 2018; Marino et al. 2018). Stellar rotation affects both the luminosity and temperature of a star, effectively changing its position in a CMD. On top of convective chemical mixing, rotating stars have rotationally induced mixing, which increases their luminosity and also their lifetimes (Maeder 2009). Moreover, rotating stars have their spherical symmetry broken due to the centrifugal forces that now act on the physical structure. These introduce a latitudinal dependence on the effective surface gravity, which is directly linked to the effective surface temperature of the star. This means that the measured colour of a rotating star changes with the stellar inclination angle. Averaged over the surface, the temperature of a rotating star is lower than that of a non-rotating star with same characteristics. This effect is thus referred to as *gravity darkening* (von Zeipel 1924). If a stellar population presents a distribution of stellar rotation rates and inclinations within its members, the aforementioned effects can cause a spread of the MSTO region of the CMD that, as mentioned in the Introduction, has been observationally found to be true in several clusters already (e.g. Bastian et al. 2018). In this context, the lack of an eMSTO in NGC 2509 may be related to the characteristics of the stellar rotation distribution of the cluster. In order to investigate this hypothesis, we present here some modelling efforts done with the MIST stellar evolution framework (Choi et al. 2016, 2018; Dotter 2016; Gossage et al. 2018), which include the effects of rotation.

We began with a qualitative analysis of the stellar rotation distribution in NGC 2509. Fixing metallicity, μ, and extinction, we visually checked how well different non-rotating and rotating MIST isochrones fit the data at different ages. The results are shown in Fig. 5. In the top panel it is apparent that the non-rotating isochrones are always too blue near the MSTO at the fixed cluster parameters, regardless of age. We varied the rotation rate of the models until we found a visual fit to the data at $\Omega/\Omega_{\rm crit,\,ZAMS} = 0.5$, where $\Omega/\Omega_{\rm crit,\,ZAMS}$ is the ratio of angular velocity at the zero-age main sequence (ZAMS), divided by the critical angular velocity of the star (see Maeder 2009 for details). At this rotation rate, the blueward bend along the upper MS (lower MSTO) in the isochrones becomes less pronounced, due to the reddening effect of gravity darkening, providing a better qualitative fit to the data. Through this initial analysis, we thus suggest that NGC 2509 might be lacking a broad range of stellar rotation rates (slow rotators in particular), and seems to be primarily composed of stars rotating near $\Omega/\Omega_{\rm crit,\,ZAMS} = 0.5$. Interestingly, this area in the blueward bend along the MS/MSTO, where the non-rotating MIST isochrones miss the data in NGC 2509, seems to be well populated in the other clusters in our sample, which would fit in the hypothesis of the MSTO spreads in these clusters as being caused by a wide range of stellar rotational velocities present, with both slow and fast rotators within the population.

There are, however, some important caveats of Fig. 5 that ought to be considered. Regarding gravity darkening, the effect is present, but it is important to note in this figure that the plotted MIST rotating isochrones have luminosity and effective temperature averaged over the stellar surface; the colour–magnitude spread due to gravity darkening and random inclination angles is not shown. It is also important to mention that the behaviour between MIST and other stellar evolution models that include rotation, such as Geneva (Ekström et al. 2012) rotating models, may differ considerably due to the different assumptions for the convective and rotational mixing

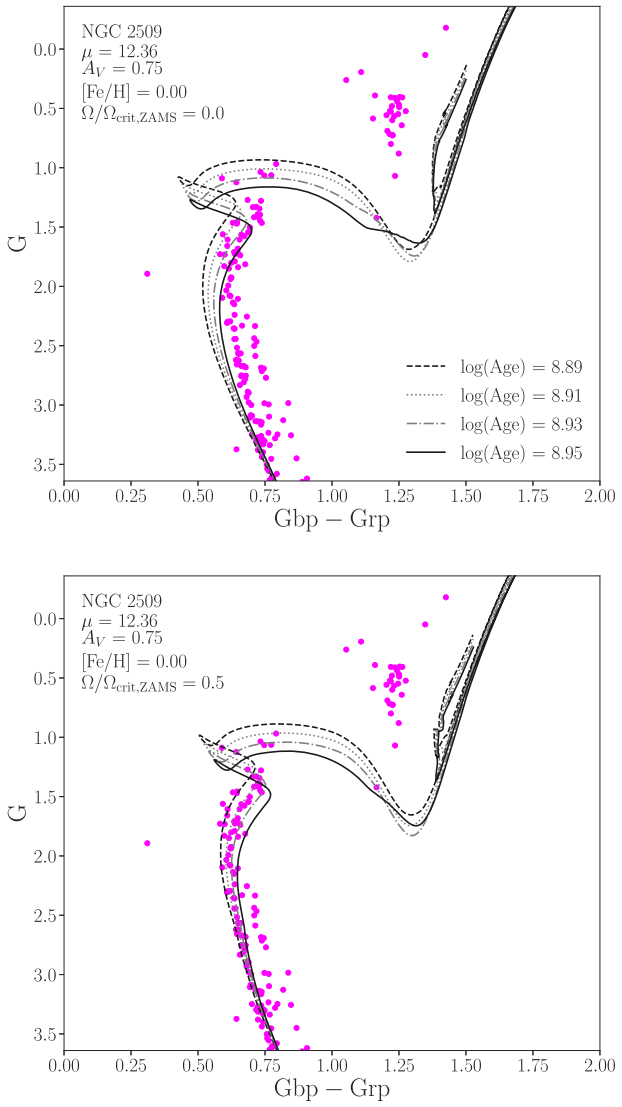

Figure 5. The observed colour–magnitude diagram (CMD) of NGC 2509 members with overplotted non-rotating (upper panel) and rotating (lower panel) isochrones for a range of ages from log(Age) = 8.89 to 8.95. The rotation rate assumed in the lower panel is our best-fitting value of $\Omega/\Omega_{crit,\,ZAMS} = 0.5$. Note that the rotating isochrones match the morphology of the upper main sequence (MS) better than the non-rotating ones.

efficiencies (Choi et al. 2016; Gossage et al. 2018). In MIST, the effect of rotational mixing is relatively low in comparison with e.g. Geneva and gravity darkening is the dominant effect, *pushing* the MSTO region of the isochrone to cooler, redder areas of the CMD.[2] However, we would like to add that we have also performed visual fits to the data with both rotating and non-rotating Geneva isochrones, finding consistent results to the ones presented here.

In either case (with or without stellar rotation), it appears that the colour–magnitude spread of turnoff stars in NGC 2509, while very narrow, still gives some uncertainty to the inferred cluster age, varying over about 75 Myr from roughly log(Age) = 8.89 to 8.95. As mentioned before, this eMSTO spread is much smaller than expected (should be near 160 Myr according to the trend presented in Niederhofer et al. 2015) for a cluster of this age.

While the visual fit of isochrones suggests that this data is best described with moderate stellar rotation of all stars in the cluster, the real constrains this qualitative analysis can put on the rotation distribution of the system are very limited. Thus, we followed it up with a dedicated statistical analysis. For this, we put our NGC 2509 data through the same simulation framework as in Gossage et al. (2018, 2019), where synthetic stellar populations are created with MATCH(Dolphin 1997, 2002), based on MIST stellar models, and are fitted to the data returning the best-fitting parameters for the observed cluster (see section 3 of Gossage et al. 2018 for a detailed description of the methodology used in this study). Gravity darkening is incorporated in these synthetic clusters considering a random distribution of inclination angles with respect to the line of sight. The fit between data and synthetic model cluster is then carried out via Hess diagrams and Poisson likelihood statistics, which are combined to find the overall likelihood of the data–model comparison between the models considered.

For our analysis, we build three different models that we refer to as σ_t, the $\sigma_t\Omega$, and the Ω models, which allow for only age spread, age spread combined with stellar rotation rate distribution within the cluster, and only stellar rotation rate distribution, respectively. We consider ages in the range of log(Age) = 7.60–9.80, and rotation rates from $\Omega/\Omega_{crit,\,ZAMS} = 0.0$ to 0.9. We then fit the *Gaia* data of NGC 2509, non-parametrically, finding that the latter two models provide a significantly better overall likelihood than the σ_t model. These two best-fitting models then score about the same probability and consistently find an extremely narrow distribution of stellar rotation rates centred at $\Omega/\Omega_{crit,\,ZAMS} = 0.5$, with the Ω model finding a best-fitting age for the cluster at log(Age) = 8.89, and the $\sigma_t\Omega$ model combining the peaked $\Omega/\Omega_{crit,\,ZAMS} = 0.5$ distribution with an age spread of 13 Myr, centred at log(Age) = 8.90, which is also consistent with no age spread whatsoever. Fig. 6 shows the 'weight' on the *y*-axis and $\Omega/\Omega_{crit,\,ZAMS}$ on the *x*-axis for these two best-fitting models, with the $\sigma_t\Omega$ and Ω models shown in the top and bottom panels, respectively. So it seems that, within the constraints of our simulation framework, the cause of the narrow MSTO in NGC 2509 is a very narrow distribution of stellar rotation rates, i.e. all stars seem to be rotating at the same rate of near $\Omega/\Omega_{crit,\,ZAMS} = 0.5$ in this cluster. Finally, we note that these simulations cannot provide tight constraints on the orientation of the rotating stars aside from saying that it is consistent with a random distribution. However, we can say that, while there is reason to think that the stellar spins may be aligned in some clusters (see Kamann et al. 2019), such an alignment could not reproduce the observed narrow MSTO in NGC 2509 by itself, i.e. a narrow $\Omega/\Omega_{crit,\,ZAMS}$ distribution is always required, according to our results.

We would like to emphasize that these simulations are here presented simply as a plausible explanation of the observed morphology of the MSTO in NGC 2509 and that the only way to confirm if stellar rotation is indeed causing this particular feature is to obtain $V \sin i$ measurements of MSTO stars in this cluster.

4.3 Binaries

Finally, we looked at the binary fraction in NGC 2509 that could also have an impact on the spread (or lack thereof) in the MSTO.

[2]We refer the reader to Choi et al. (2016, 2018), Dotter (2016), and Gossage et al. (2018) for a detailed description of the assumptions and limitations of MESA models, as well as comparisons with other stellar evolution models available.

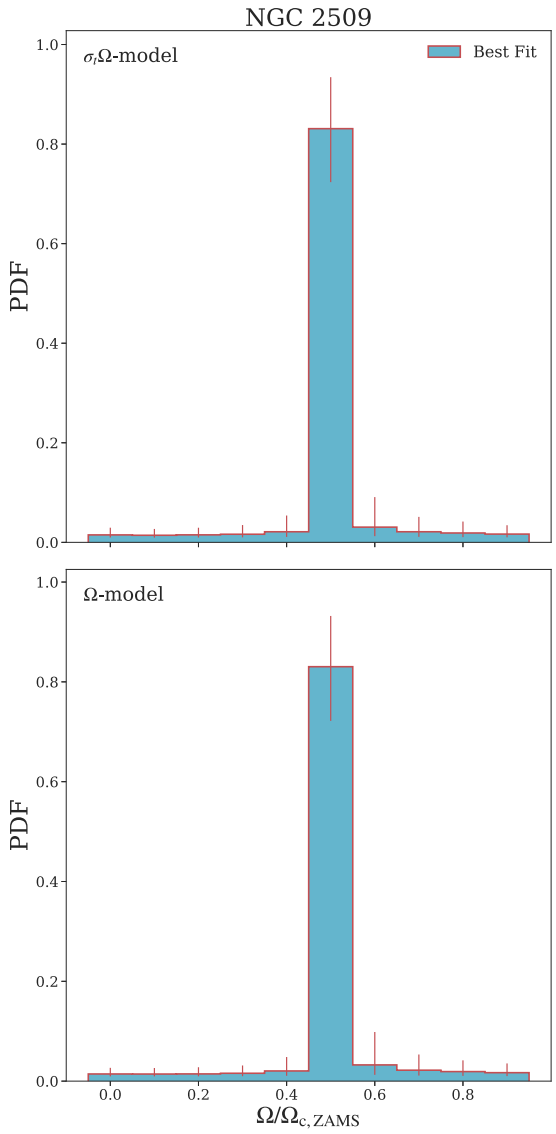

Figure 6. The resulting $\Omega/\Omega_{crit,\,ZAMS}$ distribution when employing the fit procedure of Gossage et al. (2019) for the $\sigma_t\Omega$ model (which includes an age spread and a distribution in rotation rates; in the top panel) and the Ω model (only a distribution in rotation rates; in the bottom panel). In both cases we find an extremely peaked distribution of the rotation rates. In all cases we assumed a random orientation of the stellar rotation rates with respect to the line of sight.

We define the binary fraction as

$$f_{bin} = N_{bin}/N_{tot}, \quad (1)$$

where N_{bin} is the number of members in the binary sequence along our specified MS region of each cluster, and N_{tot} is the total number of members in that same region. We define a star as member of the binary sequence when its distance to the line B in the left-hand panel of Fig. 3 is larger than 0.375 (once all peaks have been aligned with NGC 2509's one). This is approximately the inflexion or minimum point (depending on the cluster) between the two peaks of the MS distribution, separating the MS and binary sequence (vertical grey dashed line in lower right-hand panel of Fig. 3). We use the same value for all clusters that might not be exact but it is a reasonable approximation looking at our figure. The binary fractions we find following this criterion are listed in Table 1. But we need to keep in mind that these fractions are not complete, since we are only sensitive to nearly equal-mass binaries in these bands.

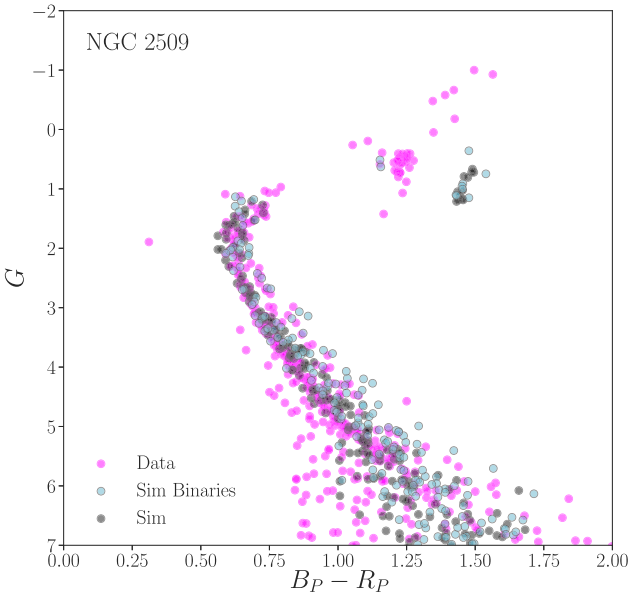

Figure 7. Colour–magnitude diagram (CMD) of both NGC 2509 data and synthetic cluster created based on our best-fitting parameters (Ω model, see text). *Gaia* data are shown as magenta filled dots, while synthetic data are shown in grey and blue filled dots, with blue dots highlighting the binaries in our synthetic population.

In order to correct for the unseen fraction of binaries in NGC 2509, we performed simulations creating synthetic clusters and comparing the synthetic CMD with the observed one. We simulated NGC 2509 assuming $M = 3100\ M_\odot$, $f_{bin} = 17$ per cent, log(Age) = 8.89, $\Omega/\Omega_{crit,\,ZAMS} = 0.5$, and a random distribution of inclination angles, as our analysis of the rotation distribution above suggests. We note that binaries are modelled in our code as having a flat mass fraction distribution (0.0–1.0), with no interaction between the stars. We then increased the binary fraction in our simulated cluster until the total number of stars in the MS region of the simulated cluster, where our observations should be complete, matches the observed number of stars in NGC 2509 in that range. We find that the fraction of binaries should be about 50 per cent, which is quite a high fraction for a cluster this age. Fig. 7 shows the CMDs of both synthetic and observed NGC 2509. The remarkable thing about this simulation is that it shows how, despite the high fraction of binaries included, these do not seem to have a broadening effect on the MSTO.

5 CONCLUSIONS

In this study, we present *Gaia* photometry of several Galactic open clusters with ages around 900 Myr and compare their MSTO morphologies. We do this by directly comparing the morphology of the MSTO region of the CMD in all clusters, instead of estimating a spread by fitting isochrones. We focus on the open cluster NGC 2509 that lacks an eMSTO while all other open clusters we could find at this age do show this feature. Through our results and analysis we arrive to the following conclusions.

(i) NGC 2509 does not show a spread in its MSTO while all other clusters at similar ages in our sample do.

(ii) The differences in morphology between NGC 2509 and other clusters are statistically significant and not likely to be caused by effects such as e.g. differential extinction. Stellar density effects on the rotation distribution of the stars in the cluster, which also could affect the width of the MSTO, are also ruled out as NGC 2509 does not seem to be any different than the others in that respect.

(iii) Stellar evolution models that include the effect of rotation are able to reproduce the particular characteristics of NGC 2509's MSTO much better than non-rotating models can. In particular, the models best fit the data when assuming a narrow range of rotational velocities centred on $\Omega/\Omega_{\rm crit,\,ZAMS} = 0.5$. This is true independently of the age and rotational inclination angle in the ranges we have tested within both MIST and Geneva frameworks.

(iv) The binary fraction we measure from observations in NGC 2509 is of $\sim$17 per cent but we are limited in that the *Gaia* bands we use are only sensitive to similar-mass binaries. We simulate the cluster based on the properties of the rotation distribution we find as a best fit in our analysis and find a total binary fraction of $\sim$50 per cent. This high fraction however does not seem to have an effect on the width of the MSTO, and so we rule out the influence of binaries as a possible cause of the big differences we see between the morphology of NGC 2509's CMD and that of the rest of clusters in our sample.

In light of these results, it is clear that NGC 2509 is a very special cluster whose unique properties could potentially reveal a great deal regarding if and how stellar rotation affects the morphology of a cluster's CMD, and, as such, it deserves further investigation. In particular, it is pressing to obtain data on the stellar rotational distribution to confirm its peaked nature. Additionally, we will be exploring our *Gaia* DR2 open cluster data base to look for other clusters with anomalous MSTOs.

ACKNOWLEDGEMENTS

MdJO, SK, CU, and NB are gratefully acknowledge funding from a European Research Council consolidator grant (ERC-CoG-646928-Multi-Pop). NB is a Royal Society University Research Fellow. Support for this work was also provided by NASA through Hubble Fellowship grant HST-HF2-51387.001-A awarded by the Space Telescope Science Institute, which is operated by the Association of Universities for Research in Astronomy, Inc., for NASA, under contract NAS5-26555.

REFERENCES

Bastian N., de Mink S. E., 2009, MNRAS, 398, L11
Bastian N. et al., 2018, MNRAS, 480, 3739
Beasor E. R. et al., 2019, MNRAS, 486, 266
Brandt T. D., Huang C. X., 2015, ApJ, 807, 25
Choi J. et al., 2016, ApJ, 823, 102
Choi J. et al., 2018, ApJ, 863, 65
Cordoni G. et al., 2018, ApJ, 869, 139
Dolphin A., 1997, New Astron., 2, 397
Dolphin A. E., 2002, MNRAS, 332, 91
Dotter A., 2016, ApJS, 222, 8
Dupree A. K. et al., 2017, ApJ, 846, L1
Ekström S. et al., 2012, A&A, 537, A146
Gossage S. et al., 2018, ApJ, 863, 67
Gossage S. et al., 2019, preprint (arXiv:1907.11251)
Kamann S. et al., 2014, A&A, 566, A58
Kamann S. et al., 2018, MNRAS, 480, 1689
Kamann S. et al., 2019, MNRAS, 483, 2197
Li C. et al., 2017, ApJ, 844, 119
Lindegren L. et al., 2018, A&A, 616, A2
Mackey A. D., Broby Nielsen P., 2007, MNRAS, 379, 151
Maeder A., 2009, Physics, Formation and Evolution of Rotating Stars. Springer-Verlag, Berlin
Marino A. F. et al., 2018, ApJ, 863, L33
Martocchia S. et al., 2018, MNRAS, 477, 4696
Niederhofer F. et al., 2015, MNRAS, 453, 2070
Piatti A. E., Bastian N., 2016, A&A, 590, A50
von Zeipel H., 1924, MNRAS, 84, 665

This paper has been typeset from a TEX/LATEX file prepared by the author.